ACS APPLIED MATERIALS & INTERFACES

Research Article

www.acsami.org

Deciphering the Metal-C_{60} Interface in Optoelectronic Devices: Evidence for C_{60} Reduction by Vapor Deposited Al

Dallas L. Matz,[§] Erin L. Ratcliff,[§] Jens Meyer,[†,‡] Antoine Kahn,[†] and Jeanne E. Pemberton*[,§]

[§]Department of Chemistry and Biochemistry, University of Arizona, Tucson, Arizona 85721, United States

[†]Department of Electrical Engineering, Princeton University , Princeton, New Jersey 08544, United States

ABSTRACT: The formation of interfacial midgap states due to the reduction of buckminsterfullerene (C_{60}) to amorphous carbon upon subsequent vapor deposition of Al is confirmed using Raman spectroscopy and X-ray, ultraviolet, and inverse photoemission spectroscopies. We demonstrate that vapor deposition of Al results in n-type doping of C_{60} due to an electron transfer from Al to the LUMO of C_{60}, resulting in the formation of midgap states near the C_{60} Fermi level. Raman spectroscopy in ultrahigh vacuum clearly identifies the presence of the C_{60} anion radical ($C_{60}^{\bullet-}$) as well as amorphous carbon created by further degradation of $C_{60}^{\bullet-}$. In contrast, the interface formed by vapor deposition of Ag shows only a slight Ag/C_{60} interfacial charge displacement with no evidence for complete metal-to-C_{60} electron transfer to form the anion radical or its further degradation products. These results confirm previous speculations of metal-induced chemical damage of C_{60} films after Al deposition, which is widely suspected of decreasing charge collection efficiency in OPVs, and provide key insight into charge collection at metal/organic interfaces in such devices.

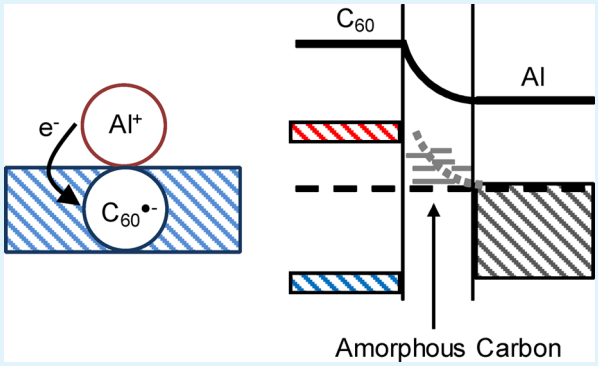

KEYWORDS: *fullerene, charge transfer, charge displacement, organic photovoltaic, Raman spectroscopy, electron spectroscopy*

1. INTRODUCTION

The electronic properties of organic/metal interfaces are of critical importance in organic electronics, as they dictate the rates of charge injection in organic light emitting diodes (OLED) and charge collection in organic photovoltaic (OPV) devices.[1−9] In the case of thin film photovoltaics, interfacial phenomena at electrode/organic interfaces can dramatically affect the distribution of electric fields vital for charge collection in the device. As an example, modeling of the photocurrent in a typical C_{60}-containing OPV has shown that the C_{60}/Al interface is a dominant contributor to electric field distribution inside the device and that this interface also contributes as an exciton dissociation site.[10]

The correlation between the properties of the metal/organic interface and OPV device performance is also reflected in the open circuit voltage (V_{OC}). Standard theory predicts that the maximum V_{OC} is given by the offset between the quasi-Fermi levels for holes and electrons. Thus, as the offset between these two levels increases during charge transport across the interface, the photovoltage increases.[11] If one ignores the effects of carrier generation and diffusion on V_{OC}, the metal−insulator−metal (MIM) model predicts the maximum V_{OC} achievable to be the work function difference between the two contacts ($\Delta\Phi_{contacts}$). This asymmetric device behavior is ideally assumed to be due to the different rates of charge injection at the two contacts into the highest occupied molecular orbital (HOMO) and lowest unoccupied molecular orbital (LUMO) of the donor and acceptor, respectively.[11−13] However, measured V_{OC} values have been shown to be extremely sensitive to the interfacial energy levels at the metal/organic interface in both planar and bulk heterojunction devices.[5,7,13−16] Therefore, in reality, the V_{OC} observed does not depend simply on $\Delta\Phi_{contacts}$; in other words, alignment of the energy levels cannot be predicted a priori and must be measured at each metal/organic interface.

Direct measurement of the energetics of the metal/organic interface have shown deviations from the ideal Schottky-Mott contact behavior.[3,4,17] Such deviations have been attributed to various interfacial phenomena that result in observed vacuum level shifts (ΔE_{vac}); these interfacial phenomena might include charge transfer, formation of interface states due to chemical reactions or metal/semiconductor proximity, or redistribution of electronic charge at the electrode surfaces.[18−21] Such interactions may affect the depletion width at the contact, altering the sharpness of the potential gradient and, thus, perturbing the electric field for charge collection.

Al/organic interfaces have become increasingly important in OPV devices, since Al is commonly used as a low work function metal for electron extraction from acceptors.[22] Previous studies of thin films of C_{60} on Al surfaces have shown the formation of a pronounced interface dipole (~0.7 eV) resulting from an electron transfer between the low work function Al and the high electron affinity (EA) C_{60} that leaves positive and negative

Received: February 19, 2013
Accepted: June 4, 2013
Published: June 4, 2013

 © 2013 American Chemical Society dx.doi.org/10.1021/am400640x | ACS Appl. Mater. Interfaces 2013, 5, 6001−6008

charges on Al and C_{60}, respectivly.[23] In this case, the metal Fermi level is essentially pinned against the C_{60} LUMO, making a contact with very little energy loss. In contrast, for devices in which Al is evaporated onto a C_{60} thin film, the resulting V_{OC} values are considerably smaller than the predicted maximum, suggesting the formation of a contact with an energy barrier between the Fermi level and LUMO.[24−28] Two possible causes have been proposed to explain these results: (i) damage of the C_{60} layer due to Al cathode evaporation and (ii) parasitic exciton quenching at the Al/organic interface.[24,29,30] It is noted, however, that these conclusions come from the indirect observation that exciton blocking layers, such as bathocuproine, result in improved device performance and not from direct evidence for charge transfer at the Al/C_{60} interface. Therefore, the goal of this work is to gain a better understanding of both the electronic structure and reaction chemistry that govern the interface of a C_{60} thin film upon vapor deposition of Al using a combination of surface Raman spectroscopy and photoelectron spectroscopy.

Raman spectroscopy has been successful in determining reaction pathways and products formed at interfaces between solid-state organics and low work function metals in previous work from this laboratory. Studies have included metallization of the organic semiconductor tris(8-hydroxyquyinoline)aluminum (Alq_3)[31,32] and smaller model molecules such as *trans*-stilbene,[33] benzene,[34,35] and pyridine[35,36] with Ag, Al, Ca, and Mg. These studies have provided considerable insight not only into the complex chemical identity of reaction products formed from low work function metal deposition but also into the mechanisms by which they form. A general theme of this reaction chemistry is metal-to-organic electron transfer leading to the formation of metal−organic adducts (Alq_3-Mg/Al/Ca, *trans*-stilbene-Al, and benzene-Mg/Al/Ag)[31−34] as well as unexpected reduction products and other chemical entities such as benzyne (benzene-Ca),[35] pyridyne (pyridine-Ca),[35] and 4,4′-bipyridine (pyridine-Mg).[36] For many systems, amorphous carbon (Alq_3-Ca/Mg/Al, benzene-Ca, and pyridine-Ca/Mg/Al)[31,32,35,36] is also observed to form through what are presumed to be radical intermediates resulting from the initial electron transfer. Given the extensive literature on the vibrational spectroscopy of fullerenes,[37−40] including many studies on the reaction and intercalation of reactive metal species with C_{60},[41−45] Raman spectroscopy is an excellent choice of technique for characterization of reaction chemistry at the Al/C_{60} interface. These two classes of techniques, vibrational and electron spectroscopies, provide a powerful combination with which to fully elucidate the chemical and electronic nature of the Al/C_{60} interface.

2. EXPERIMENTAL SECTION

2.1. Materials. Ag sample stubs were machined in-house from 12.5 mm dia polycrystalline Ag rods (99.9985%, Alfa Aesar). These substrates were mechanically and chemically polished according to previously described procedures.[46] Smooth, clean substrates so produced were mounted in stainless steel holders and introduced into the vacuum chamber through a load lock chamber and outgassed overnight at pressures $<1 \times 10^{-6}$ Torr. After thorough outgassing, the samples were transferred to a closed-cycle liquid He-cooled cryogenic arm (DE-204B, Advanced Research Systems) and cooled to 150 K. The substrate temperature was monitored and maintained with a cryogenic temperature controller (Model 34, Cryo-Con) and a K-type thermocouple mounted in close proximity to the sample holder.

C_{60} (99+%, MER Corporation) was vacuum-sublimed three times prior to use. C_{60} was outgassed at 400 K at pressures $\leq 1 \times 10^{-9}$ Torr for 1 h. 50 Å thick films (6.6×10^{14} molecules/cm^2) were deposited from a Knudsen cell using 2−2.5 A of current at 600 K, resulting in a rate of 0.5 Å/s.

Al or Ag metal films were postdeposited onto these C_{60} films from Al_2O_3-coated Ta boats (ME9-A0-M0-M5, R. D. Mathis Co.) in 5 Å increments (2.0×10^{15} atoms/cm^2 of Ag and Al, assuming bulk metal densities) up to 20 Å in mass thickness. All film thicknesses were monitored using a quartz crystal microbalance and thickness monitor (Model TM-400, Maxtek Inc.) cooled to liquid N_2 temperatures to ensure a sticking coefficient of unity. Metal film thicknesses are reported as mass thickness values throughout. Al wire (Sigma-Aldrich, 99.999%) and Ag foil (Sigma-Aldrich, 99.9%) were slowly outgassed at pressures $<10^{-8}$ Torr until they melted, formed a ball, and began to evaporate (~8 h).

H_2SO_4 (EMD, 98%), $HClO_4$ (EMD, 70%), HCl (EMD, 37%), CrO_3 (Alfa Aesar, 98+%), and NH_4OH (EMD, 28−30%) were used as received. Water (>18 MΩ resistivity, <8 ppb total organic content) was purified using a Waters Milli-Q UV Plus purification system.

2.2. Instrumentation. All thin films (C_{60}, Al, Ag) used in these experiments were deposited and subsequently analyzed in a custom-built ultrahigh vacuum (UHV) chamber described previously.[31,32] Base pressures for surface preparation were maintained at $<3 \times 10^{-10}$ Torr with working pressures never exceeding 10^{-9} Torr. The working pressure of the sample analysis chamber was maintained at or below 5×10^{-11} Torr.

Raman spectroscopy was performed using the previously described optical arrangement[32,35] consisting of a Nd:YVO_4 diode laser (Coherent Verdi 2W) excitation source at 532 nm and a single monochromator system with a spectral bandpass of 5 cm^{-1} utilizing a Newton EM-CCD detector (Andor Technology DU971P−BV.) The laser radiation was made p-polarized with respect to the plane of incidence using a CVI Laser Optics Fresnel rhomb half-wave retarder and was incident on the surface with a power of typically 25−30 mW in a ~1.2 mm dia spot. The resulting excitation power density of ~2 W/cm^2 is well below the flux of ~5 W/cm^2 required for photopolymerization as previously reported by Rao et al.[47]

Spectral peak fitting was performed using 100% Gaussian peaks. Peak frequencies for C_{60} were fit on the basis of frequencies from Dong[48] (±5 cm^{-1}), with fwhm values of 15 cm^{-1} (±10 cm^{-1}) and relative intensities of ±20%. Amorphous carbon product modes were fit using four broad bands with peak frequencies (±20 cm^{-1}), fwhm, and relative intensities (±50%) as outlined by Ferrari and Robertson.[49] Reaction product bands were fit with single broad peaks and were allowed to vary in frequency by ±15 cm^{-1}, fwhm by ±50 cm^{-1}, and intensity by ±50%. Fits were deemed acceptable for χ^2 values >0.99.

XPS, UPS, and IPES measurements were carried out in a UHV chamber with base pressure of ~10^{-10} Torr. The He I (21.22 eV) and He II (40.8 eV) photon lines from a discharge lamp were used in UPS, with an experimental resolution of 0.15 eV. IPES was operated in the isochromat mode using a previously described setup.[50] The resolution in the IPES measurements was 0.45 eV. The Fermi level reference was established for both UPS and IPES measurements on a freshly evaporated Au surface. XPS was done with the Al Kα line of a dual anode source, with a resolution of 0.8 eV.

3. RESULTS AND DISCUSSION

3.1. Raman Spectroscopy. Previous studies of Al deposition onto organic thin films from this laboratory[31,36] have shown that reaction chemistry is initiated by electron transfer, leading to the formation of amorphous carbon (a-C). C_{60} behaves as an electron acceptor and can form anion radicals with up to six electrons.[51] Both solution phase Raman spectroelectrochemistry[52,53] and C_{60} alkali metal doping experiments[54−56] have correlated a shift to lower frequency of the A_g (2) mode (1467 cm^{-1} in the pristine film) to reduction of C_{60} (i.e., formation of C_{60} radical anions). The magnitude of this shift can be used as a semiquantitative measure of the number of electrons transferred to C_{60}, with a 6−7 cm^{-1}

decrease in frequency of this band per electron transferred per C_{60}.

The Raman spectrum of a pristine 5 ML film (50 Å) of C_{60} at 150 K is shown by the black lines in Figures 1a and 2a. A

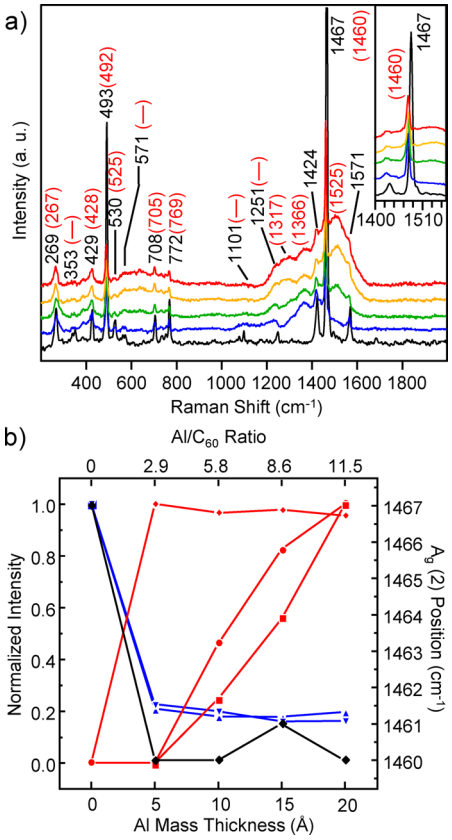

Figure 1. (a) Raman spectra for a pristine 5-ML C_{60} film before (black) and after deposition of 5 (blue), 10 (green), 15 (gold), and 20 (red) Å of Al with inset of the region around 1467 cm^{-1} showing the shift in the A_g (2) mode. (b) Normalized Raman intensity as a function of Al coverage for the C_{60} A_g (1) mode at 493 cm^{-1} (blue triangle), the C_{60} A_g (2) mode at 1460 cm^{-1} (inverted blue triangle), the a-C D-band at 1317 cm^{-1} (red square), the a-C G-band at 1525 cm^{-1} (red circle), and the reaction product band at 1366 cm^{-1} (red diamond). The position of the A_g (2) mode (black diamond) as a function of Al coverage is plotted on the right axis.

summary of peak frequencies and assignments for C_{60} and its reaction products can be found in Table 1. Fifteen bands in this spectrum are assigned to C_{60} including two nondegenerate A_g modes (near 495 and 1467 cm^{-1}) and eight 5-fold degenerate H_g modes (near 269, 428, 708, 772, 1100, 1250, 1423, and 1572 cm^{-1}).[42,48] The remaining four bands are assigned as combination modes, the [H_g (4) − H_g (2)] at 350 cm^{-1}, the [G_g (3) + H_g (1)] at 1082 cm^{-1}, the [H_g (2) + H_g (6)] at 571 cm^{-1}, and one additional F_{1u} band at 533 cm^{-1} which is not normally Raman active. Several of these modes appear as overlapping doublets in the spectrum due to activation of normally Raman-inactive modes due to the broken symmetry caused by the presence of ^{13}C.[48] The frequencies of all bands observed are consistent with those reported previously for C_{60} films, demonstrating that no reaction chemistry occurs between C_{60} and the underlying Ag substrate.[37−40]

Figure 1a also shows Raman spectra for this C_{60} film after vapor deposition of 5 (blue), 10 (green), 15 (gold), and 20 Å

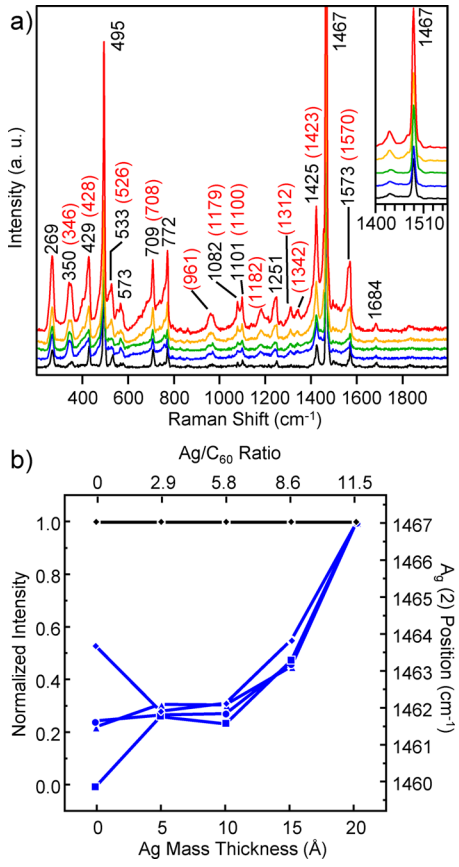

Figure 2. (a) Raman spectra for a pristine 5-ML C_{60} film before (black) and after deposition of 5 (blue), 10 (green), 15 (gold), and 20 (red) Å of Ag with inset of the region around 1467 cm^{-1} showing the lack of shift in the A_g (2) mode. (b) Normalized Raman intensity as a function of Ag coverage for the C_{60} A_g (2) mode at 1467 cm^{-1} (blue diamond), H_g (3) mode at 709 cm^{-1} (blue square), H_g (1) mode at 269 cm^{-1} (blue triangle), and G_u (4) + H_u (1) combination band at 1312 cm^{-1} (blue circle). The position of the A_g (2) mode (black diamond) as a function of Ag coverage is plotted on the right axis.

(red) of Al. Although some spectral characteristics of the native C_{60} film are maintained, new spectral features can also be distinguished: three new broad bands of moderate intensity at 1317, 1366, and 1525 cm^{-1} and a weak, broad band centered near 600 cm^{-1}. Three of these new bands (600, 1317, and 1525 cm^{-1}) are only seen for Al thicknesses of 10 Å or higher. In addition, the four low intensity modes of the native C_{60} at 353, 571, 1101, and 1251 cm^{-1} become indistinguishable from the noise at progressively higher Al thicknesses, most likely due to the formation of an opaque overlayer of Al. One additional spectral feature of note is the shift of the A_g (2) mode of C_{60} from 1467 to 1460 cm^{-1} for all Al thicknesses. As noted above, this shift of 7 cm^{-1} corresponds to an average of one electron per C_{60} transferred from Al in this composite film. Nishinaga et al. showed a similar one-electron transfer from Ge to C_{60} when the two were codeposited via molecular beam epitaxy; their resulting composite film was also shown to have semiconducting properties.[41]

For Al thicknesses greater than 5 Å, broad bands appear at 1317 and 1525 cm^{-1}; these are assigned to the D and G bands, respectively, of amorphous carbon (a-C).[49,57,58] As a result, spectral fitting of these C_{60}/Al spectra can be performed to provide further insight into the nature of the a-C formed. This was accomplished here using the fitting procedure outlined by

Table 1. Raman Peak Frequencies and Assignments for a 5 ML C_{60} Thin Film before and after Ag and Al Deposition

frequency (cm^{-1})			
pristine C_{60}	C_{60} with 20 Å Al	C_{60} with 20 Å Ag	assignments[a,b]
269	267	269	H_g (1)
		341	H_u (1)
350		346	H_g (4) − H_g (2)
		402	G_u (1)
429	428	428	H_g (2)
495	492	495	A_g (1)
533	525	526	F_{1u} (1)
		551	2 × H_g (1)
573	569	573	F_{2g} (1)
		682	2 × H_u (1)
709	705	708	H_g (3)
772	769	772	H_g (4)
		794	2 × G_u (1)
		825	H_g (5) − H_g (1)
		861	2 × H_g (1)
		961	G_u (1) + H_u (2)
1079		1079	G_g (3) + H_g (1)
1101		1100	H_g (5)
		1140	H_g (2) + H_g (4)
		1182	F_{1u} (3)
		1211	A_g (1) + H_g (3)
1251		1251	H_g (6)
		1270	A_g (1) + H_g (4)
	1317		a-C (D-Band)
		1312	G_u (4) + H_u (1)
		1342	F_{2g} (3) + H_g (2)
	1366		unidentified reaction product
		1406	F_{1g} (2) + H_g (1)
1425	1424	1423	H_g (7)
1467	1460	1467	A_g (2)
	1525		a-C (G-Band)
1573	1571	1570	H_g (8)
1684		1684	H_g (2) + H_g (6)

[a] C_{60} assignments taken from ref 48. [b] Amorphous carbon assignments based on ref 49.

Ferrari and Robertson[49] that requires two Gaussian bands to fit the D band (near 1249 and 1317 cm^{-1}) and the G band (near 1450 and 1525 cm^{-1}). Although the most rigorous curve fitting treatment for a-C utilizes an asymmetric Breit-Wigner-Fano (BWF) line shape,[59−61] it has been shown that use of two simple Gaussians for each of the D and G bands adequately accounts for the asymmetric line shape observed in the spectra of carbon films.[49,57,58]

From these fits, an integrated peak area ratio of the D to G bands, $I(D)/I(G)$, of 0.2 is obtained for Al thicknesses >5 Å. In conjunction with this value, the G band peak frequency of 1525 cm^{-1} suggests that the a-C is predominantly sp^2 in nature with only ∼20% sp^3 character.[49] In addition to the D and G bands, a weak, broad band is seen near 600 cm^{-1}, characteristic of hydrogen-free a-C.[57] It is noted that similar carbonaceous products have been observed previously in reactions of liquid Al infiltration of C_{60} powder at 750 °C under reduced pressure.[62] In this study, domains of nanocrystalline graphite (0% sp^3 character) were identified using transmission electron microscopy and Raman spectroscopy. In a related study by Nishinaga in which Al and C_{60} were codeposited,[41] insulating films were reported that were likely due to decomposition of C_{60} to a-C as reported here; however, the presence of a-C was not substantiated by Raman spectroscopy in this study.

Figure 1b shows plots of normalized Raman intensities for five spectral bands as a function of Al coverage: two bands represent the behavior of unreacted C_{60}, the A_g (1) band at 493 cm^{-1} and the A_g (2) band at 1467 cm^{-1}, and three bands at 1366 (discussed below), 1317, and 1525 cm^{-1} (a-C) represent the behavior of the reaction products. The intensities in these plots are normalized to the highest intensity observed for each band across the range of Al thicknesses studied, including zero Al coverage. The decrease in normalized intensity of the native C_{60} bands and the increase in normalized intensity of the reaction product bands confirm the consumptive conversion of C_{60} into reaction products, including a-C, since the product bands increase at the expense of the native C_{60} bands.

One final spectral feature of note is the broad band at 1366 cm^{-1}, which is observed most clearly at an Al thickness of 5 Å. This band clearly indicates that reaction chemistry has occurred, but a definitive assignment for this band has not been achieved. One possible explanation is the broadening and shift to lower frequencies of F_{1u} (4) modes, which are normally only IR-active but which may become Raman active in the spectrum due to broken inversion symmetry upon metal deposition.[63] These bands have been previously observed in the IR spectrum of RbC_{60} and CsC_{60} powders produced by cosublimation[64] and were attributed to metallo-fulleride polymers. However, no other normally IR-active bands are observed in these Raman spectra, possibly due to spectral overlap of the Raman active and IR active modes. This explanation is also inconsistent with the large intensity of this band in the spectra in Figure 1a. The only other spectral evidence in support of polymerization is the broadening observed near the A_g (2) mode at 1460 cm^{-1}, which can be seen clearly in the spectrum of C_{60} after deposition of 5 Å Al. Similar broadening has been observed in Raman spectra from metallo-fulleride polymers.[64−66] However, this explanation does not rationalize the high intensity of the 1366 cm^{-1} band. In total, the evidence for polymerization is, at best, inconsistent and incomplete, thereby precluding definitive assignment of the 1366 cm^{-1} band to metallo-fulleride polymer formation.

In addition to the proposed electron transfer mechanism, other possible explanations for the observed reaction chemistry include photochemical reaction by the incident laser beam and thermal reaction by the hot evaporated Al atoms. The lack of any apparent chemistry of the pristine C_{60} film greatly decreases the probability of any laser-induced photochemical reaction chemistry upon deposition of Al onto C_{60},[67] further supporting our proposed metal-to-C_{60} electron transfer mechanism. However, additional evidence is needed to eliminate thermal reaction as an explanation for the results with Al.

Previous studies in this laboratory have shown vapor deposited Ag to be more inert toward metal-to-organic electron transfer than Al.[31,34,36] This difference in reaction chemistry can be exploited to provide useful control experiments to further support the proposed electron transfer reaction pathway. If this chemistry is in fact due to Al-to-C_{60} electron transfer and Ag is unreactive toward this electron transfer reaction, deposition of Ag should not result in formation of either $C_{60}^{\bullet-}$ or a-C. These control experiments were conducted as follows.

Figure 2a shows spectra from a 5 ML C_{60} thin film before (black trace) and after vapor deposition of 5 (blue), 10 (green),

15 (gold), and 20 Å (red) of Ag. Deposition of Ag does result in the appearance of new bands not observed in the spectrum of the pristine film, but significantly, none of these new bands is attributable to a-C and the lack of any frequency shift in the A_g (2) band substantiates the assertion that degradation of the C_{60} film is *not* due to thermal reactions induced by hot evaporated metal atoms. Given that the evaporation temperature of Ag is almost 200 K higher than that of Al,[68] rendering the evaporated Ag atoms more energetic than the correspondingly evaporated Al atoms, the absence of any reaction chemistry with Ag suggests that thermally induced reactions do not occur.

The new bands observed upon Ag deposition accompany an overall increase in spectral intensity for all bands suggesting surface enhancement (SERS) from Ag nanoparticles on the C_{60} film surface. The new bands include 12 overtone/combination bands, another characteristic of SERS of these systems,[69−72] the $[2 \times H_g (1)]$ at 551 cm^{-1}, the $[2 \times H_u (1)]$ at 682 cm^{-1}, the $[2 \times G_u (1)]$ at 794 cm^{-1}, the $[H_g (5) - H_g (1)]$ at 825 cm^{-1}, the $[2 \times H_g (2)]$ at 861 cm^{-1}, the $[G_u (1) + H_u (2)]$ at 961 cm^{-1}, the $[H_g (2) - H_g (3)]$ at 1140 cm^{-1}, the $[A_g (1) + H_g (3)]$ at 1211 cm^{-1}, the $[A_g (1) + H_g (4)]$ at 1270 cm^{-1}, the $[G_u (4) + H_u (1)]$ at 1312 cm^{-1}, the $[F_{2g} (3) + H_g (2)]$ at 1342 cm^{-1}, and the $[F_{1g} (2) + H_g (2)]$ at 1406 cm^{-1}. Three normally Raman-inactive modes are also observed, the H_u (1) mode at 341 cm^{-1}, the G_u (1) mode at 402 cm^{-1}, and the F_{1u} at 1182 cm^{-1} (see Table 1).[48] Figure 2b shows plots of normalized intensity of four bands representative of the behavior of the C_{60} bands as a function of Ag thickness. Three of these bands, the H_g (1) at 269 cm^{-1}, the H_g (3) at 709 cm^{-1}, and the A_g (2) at 1467 cm^{-1}, are normal Raman modes for C_{60} and are observed prior to Ag deposition. However, one band, the $[G_u (4) + H_u (1)]$ at 1312 cm^{-1}, is a combination band not observed in the pristine C_{60} film without SERS.

Almost all bands exhibit a significant increase in intensity by a factor of ∼3.5 for a Ag thickness of 20 Å due to SERS.[69−72] Although previous work on the SERS behavior of thin films of C_{60} deposited onto noble metals has been published,[69−71] no previous work on the postdeposition of Ag onto thin films of C_{60} has been reported. Interestingly, the intensity variations of the A_g (2) band deviate slightly from those of the other bands. The A_g (2) band shows a slight decrease in intensity after deposition of the first 5 Å of Ag followed by enhancement of the intensity at higher Ag thicknesses. This difference in behavior appears to be due to the convolution of band symmetry effects with surface enhancement, since the two A_g (1) combination modes $[A_g (1) + H_g (3)]$ and $[A_g (1) + H_g (4)]$ at 1211 and 1270 cm^{-1}, respectively, are also unusually low in intensity.

The absence of both a frequency shift of the A_g (2) mode and new bands attributable to reaction products clearly indicate that reaction chemistry similar to that observed for Al deposition on C_{60} does not occur with Ag. Nonetheless, a more subtle change in the C_{60} spectrum in the form of band broadening throughout the spectrum is observed and, as explained below, does indicate some electronic changes in the C_{60} film upon Ag deposition. In fact, the observed spectral broadening can result from multiple contributions. One predominant source of asymmetric broadening to the low frequency side of many of the C_{60} bands arises from the natural abundance of ^{13}C (1.108%) and its consequent effect on peak frequencies. ∼66% of the C_{60} molecules in the film exist as $^{13}C^{12}C_{59}$ leading to a second pronounced set of peaks at slightly lower frequency. This source of broadening would be expected to be the same for films with Ag and Al. A second source of broadening is the asymmetric low frequency broadening which has previously been observed in SERS spectra of C_{60} deposited onto roughened noble metal surfaces.[53,72,73] Broadening of this nature can be seen through the entire spectrum upon deposition of Ag onto C_{60} (Figure 2a) in close agreement with previous C_{60} SERS studies. This additional contribution to broadening is thought to be due to interaction of the π^* electron levels of C_{60} with the 4d electron density of the Ag nanoparticles, which is predicted to result in a frequency decrease due to partial population of the π^* levels.[48,70,73,74] The weak Ag−C_{60} interaction can be viewed as a partial charge displacement from Ag to C_{60}, in agreement with previous UPS studies of C_{60} thin films (0.25−2 ML) deposited onto Ag.[70,75] It was determined in these previous studies that, although the electronic structure of C_{60} remains essentially unchanged, new interfacial electronic states arise in the HOMO−LUMO band gap of C_{60} that signify a substantial interfacial interaction between Ag and C_{60}. These previous photoelectron measurements are further substantiated by ab initio calculations that show a small 0.2 electron per C_{60} transfer from Ag to C_{60}.[76]

In total, the difference in reactivity observed for these two metals can be explained by consideration of the electronegativity of the metal adlayers: 1.5 eV (Al) versus 1.9 eV (Ag).[68] This suggests that the Ag atoms or metal clusters are less likely to exchange electrons with the C_{60} film. Figure 3 is a schematic that illustrates the proposed differences in interaction for the two metals. Figure 3a indicates the picture for Al in which Al^+ and $C_{60}^{\bullet-}$ as an interfacial salt are formed as the result of complete metal-to-C_{60} electron transfer. Figure 3b illustrates the case of charge displacement for Ag in which electron density from Ag is delocalized into new interfacial electronic states of the C_{60} film without formal electron transfer.

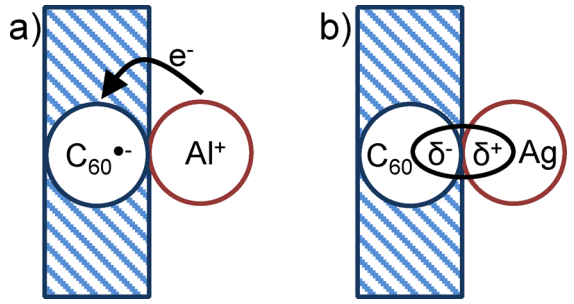

Figure 3. Schematic of the proposed interactions between C_{60} thin films and vapor deposited metals. (a) Al-to-C_{60} charge transfer resulting in formation of $C_{60}^{-\bullet}/Al^+$ salt and (b) charge displacement altering the electronic states of both Ag and C_{60}.

3.2. Electron Spectroscopy. In light of the clear evidence for the presence of a-C and electron transfer at the C_{60}/Al interface, we can consider the energetics with new insight. Figure 4a shows the UPS results for a 100 Å film of C_{60} before and after deposition of 2 and 5 Å Al, and Figure 4b displays the IPES spectra for the 100 Å C_{60} film before and after deposition of 5 Å Al. Figure 4c shows the carbon (C 1s) XPS spectra for the same films represented in Figure 4a. The UPS data for the C_{60} film in Figure 4a has an onset of states at −1.4 eV below the Fermi level while the IPES data in Figure 4b has the onset of unoccupied states beginning at ∼0.8 eV above the Fermi level. The electronic gap, which is relevant for charge transfer

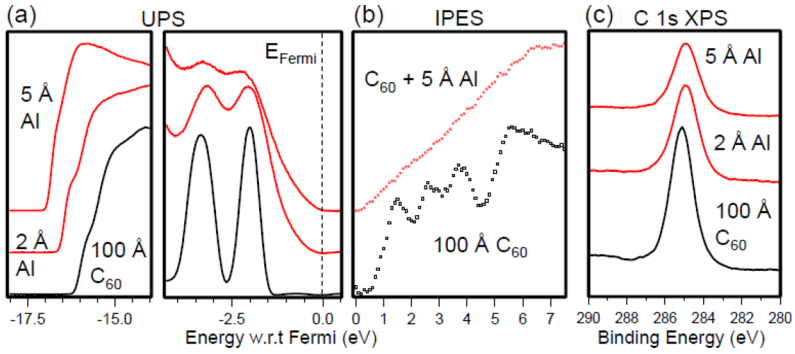

Figure 4. Electron spectroscopy for a 100 Å C_{60} film before (black) and after (red) Al depositions: (a) ultraviolet photoelectron, (b) inverse photoemission, and (c) X-ray photoelectron spectra.

between C_{60} and Al,[3,8,9,22] is the difference between the onsets of HOMO and LUMO of the C_{60} and, from these data, is estimated to be 2.2 eV. The separation between the first and second HOMO peaks is 1.35 eV in Figure 4a, with an average fwhm of 0.6 eV, consistent with previous reports by Lichtenberger et al.[77] In the XPS spectrum in Figure 4c, a single, narrow peak is observed for the C_{60} C 1s at 285.1 eV.[77] Figure 5a gives the energy band diagram for a film of C_{60} and Al, assuming vacuum level alignment (i.e., the materials have not equilibrated via interface formation).

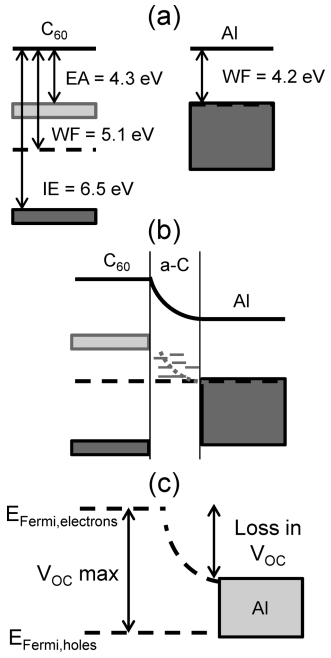

Figure 5. Energy band diagrams of the C_{60}-Al interface. (a) Before interface formation, assuming vacuum level alignment; (b) electrons flow from the Al to the C_{60} to reach thermal equilibrium; (c) impact of interfacial charge transfer on the open circuit voltage in an organic photovoltaic.

Previous reports of photoemission studies of C_{60} with various metals of different work function have concluded that the Fermi levels of both the C_{60} film and the substrate align upon formation of the interface.[78,79] Given that the Fermi level position of bulk Al is closer to the vacuum level than the C_{60} LUMO, one would expect LUMO level mixing with Al states, with little change to the HOMO of the C_{60}. Electrons are expected to flow from the Al to the C_{60} (reduction of the C_{60} film), causing a shift of the vacuum level as the system reaches thermal equilibrium (Figure 5b).

As shown by the Raman spectral results (Figure 1), charge transfer reactions within the film are complete after deposition of the first 5 Å of Al. For the 5 ML C_{60} films studied here, the entire C_{60} film is reduced by one electron with only 5 Å of Al deposited on the basis of the full 6−7 cm^{-1} shift observed in the A_g (2) mode. This result suggests that the Al atoms penetrate the entire depth of this 5 ML film. Results by Weaver also suggest that Al penetrates a C_{60} film, indicating that the interfacial region is a unique phase.[80] Upon deposition of Al, the photoemission cutoff (left panel of Figure 4a) shows a shift that indicates a lowering of the vacuum level (i.e., decrease in the work function), consistent with a decrease in electron density on the metal side of the interface, i.e., possible partial electron transfer to the C_{60} molecules.[4] The energy window near the Fermi level shows a significant change in the density of states of the C_{60} film, with broadening and extension of states to near the Fermi level, consistent with partially or fully reduced C_{60}.[80,81] The separation between the first and second HOMO peaks is still on the order of 1.3 eV, indicating little change to the valence structure of the C_{60} film. Previous reports have also demonstrated a broadening of the HOMO peaks, which has been suggested to be due to two unique environments probed by PES: (i) the Al/C_{60} charge transfer and (ii) bulk C_{60}.[80] The IPES data in Figure 4b show a continuum of empty states associated with Al and the Al−C_{60} system, which extend to the Fermi level. The C 1s peak of C_{60} in Figure 4c shifts by 0.2 eV toward lower binding energies, consistent with an increase in negative charge density in the near-surface region of the C_{60} film as well as with the small shift observed in the valence spectra. The fwhm of the peak also increases significantly from ∼0.9 to 1.2 eV, which has been reported for amorphous carbon species,[82] consistent with the Raman spectral results. Reports of C_{60} deposited onto Al substrates have linked shifts in the C 1s binding energy with electronic interactions confined to the first layer of C_{60} on Al.[83] A similar shift in binding energy was also observed by Ohno et al., with a calculated charge transfer of 0.2 electrons per C_{60} molecule from the Al film.[83]

Figure 5c shows the result of the interfacial charge transfer on the open circuit voltage. The blending of the C_{60} LUMO with nearest neighbor Al atoms due to charge transfer results in the formation of localized a-C. The presence of this a-C phase represents a localized energetic step that decreases the separation between the Fermi level for holes and electrons at the electron-extracting contact, leading to a reduction in

photovoltage. Intercalation of Al into the C_{60} film further hinders electron extraction, leading to a further decrease in open-circuit voltage. In fact, there have been multiple reports of electrical shorts in C_{60}-Al devices, with open-circuit voltages on the order of 10 mV.[84,85]

4. SUMMARY

In conclusion, the properties that make C_{60} a favorable material for use as a molecular acceptor layer (i.e., n-type semiconductor) also allow it to accept electrons from evaporated Al during device fabrication. This electron transfer initiates degradation chemistry of the C_{60} film into a $Al^{+}/C_{60}^{\bullet-}$ salt and a-C. The presence of these reaction products leads to the formation of proposed interfacial gap states in the energy region between the C_{60} HOMO and LUMO. These states are directly observed in electron spectroscopy, and their presence alters the energetics of charge collection at the metal/organic interface, contributing to less than ideal device performance.

AUTHOR INFORMATION

Corresponding Author

*E-mail: pembertn@u.arizona.edu. Phone: (520) 621-8245. Fax: (520) 621-8248.

Present Address

‡Philips Research, Weisshausstrasse 2, Aachen, Germany.

Notes

The authors declare no competing financial interest.

ACKNOWLEDGMENTS

Research was supported as part of the Center for Interface Science: Solar-Electric Materials (CIS:SEM), an Energy Frontier Research Center funded by the U.S. Department of Energy, Office of Basic Energy Sciences under Award Number DE-SC0001084. The UHV Raman spectroscopy instrumentation used for this work was developed under funding from the National Science Foundation through grant awards CHE-0317114 and CHE-0848624.

REFERENCES

(1) Aoki, M.; Toyoshima, S.; Kamada, T.; Sogo, M.; Masuda, S.; Sakurai, T.; Akimoto, K. *J. Appl. Phys.* **2009**, *106*, 043715.

(2) Bhatt, M. D.; Suzuki, S.; Sakurai, T.; Akimoto, K. *Appl. Surf. Sci.* **2010**, *256*, 2661−2667.

(3) Cahen, D.; Kahn, A. *Adv. Mater.* **2003**, *15*, 271−277.

(4) Ishii, H.; Sugiyama, K.; Ito, E.; Seki, K. *Adv. Mater.* **1999**, *11*, 605−625.

(5) Mihailetchi, V. D.; Blom, P. W. M.; Hummelen, J. C.; Rispens, M. T. *J. Appl. Phys.* **2003**, *94*, 6849−6854.

(6) Mitrasinovic, P. M. *Curr. Org. Chem.* **2010**, *14*, 198−211.

(7) Ramsdale, C. M.; Barker, J. A.; Arias, A. C.; MacKenzie, J. D.; Friend, R. H.; Greenham, N. C. *J. Appl. Phys.* **2002**, *92*, 4266−4270.

(8) Zhu, X. Y. *Annu. Rev. Phys. Chem.* **2002**, *53*, 221−247.

(9) Zhu, X. Y. *J. Phys. Chem. B* **2004**, *108*, 8778−8793.

(10) Pettersson, L. A. A.; Roman, L. S.; Inganas, O. *J. Appl. Phys.* **1999**, *86*, 487−496.

(11) Hoppe, H.; Sariciftci, N. S. *J. Mater. Res.* **2004**, *19*, 1924−1945.

(12) Parker, I. D. *J. Appl. Phys.* **1994**, *75*, 1656−1666.

(13) Brabec, C. J.; Cravino, A.; Meissner, D.; Sariciftci, N. S.; Fromherz, T.; Rispens, M. T.; Sanchez, L.; Hummelen, J. C. *Adv. Funct. Mater.* **2001**, *11*, 374−380.

(14) Barker, J. A.; Ramsdale, C. M.; Greenham, N. C. *Phys. Rev. B* **2003**, *67*, 075205.

(15) Brabec, C. J.; Cravino, A.; Meissner, D.; Sariciftci, N. S.; Rispens, M. T.; Sanchez, L.; Hummelen, J. C.; Fromherz, T. *Thin Solid Films* **2002**, *403*, 368−372.

(16) Cheyns, D.; Poortmans, J.; Heremans, P.; Deibel, C.; Verlaak, S.; Rand, B. P.; Genoe, J. *Phys. Rev. B* **2008**, *77*, 165332.

(17) Sakurai, T.; Toyoshima, S.; Kitazume, H.; Masuda, S.; Kato, H.; Akimoto, K. *J. Appl. Phys.* **2010**, *107*, 043707.

(18) Hoelzel, J.; Schulte, F. K.; Wagen, H. *Solid State Surface Physics*; Springer: Berlin, 1979.

(19) Slater, J. C.; Frank, N. H. *Electromagnetism*; Dover Publications: New York, 1969.

(20) Nielsen, P. *Photogr. Sci. Eng.* **1974**, *18*, 186−197.

(21) Woodruff, D. P.; Delchar, T. A. *Modern Techniques of Surface Science*; Cambridge University Press: Cambridge, 1994.

(22) Hill, I. G.; Kahn, A.; Soos, Z. G.; Pascal, R. A. *Chem. Phys. Lett.* **2000**, *327*, 181−188.

(23) Seo, J. H.; Kang, S. J.; Kim, C. Y.; Cho, S. W.; Yoo, K. H.; Whang, C. N. *Appl. Surf. Sci.* **2006**, *252*, 8015−8017.

(24) Peumans, P.; Bulovic, V.; Forrest, S. R. *Appl. Phys. Lett.* **2000**, *76*, 2650−2652.

(25) Oh, H. S.; Lee, J. U.; Lee, W. J.; Jang, K. U.; Ahn, J. H.; Lee, D. K.; Lee, H. S.; Kim, T. W. *J. Korean Phys. Soc.* **2006**, *48*, 1488−1491.

(26) Rand, B. P.; Li, J.; Xue, J. G.; Holmes, R. J.; Thompson, M. E.; Forrest, S. R. *Adv. Mater.* **2005**, *17*, 2714−2718.

(27) Huang, J.; Yu, J. S.; Lin, H.; Jiang, Y. D. *J. Appl. Phys.* **2009**, *105* (7), 073105.

(28) Hur, S. W.; Oh, H. S.; Oh, Y. C.; Chung, D. H.; Lee, J. U.; Park, J. W.; Kim, T. W. *Synth. Met.* **2005**, *154*, 49−52.

(29) Arbour, C.; Armstrong, N. R.; Brina, R.; Collins, G.; Danziger, J.; Dodelet, J. P.; Lee, P.; Nebesny, K. W.; Pankow, J.; Waite, S. *Mol. Cryst. Liq. Cryst.* **1990**, *183*, 307−320.

(30) Hirose, Y.; Kahn, A.; Aristov, V.; Soukiassian, P.; Bulovic, V.; Forrest, S. R. *Phys. Rev. B* **1996**, *54*, 13748−13758.

(31) Davis, R. J.; Pemberton, J. E. *J. Phys. Chem. C* **2008**, *112*, 4364−4371.

(32) Davis, R. J.; Pemberton, J. E. *J. Am. Chem. Soc.* **2009**, *131*, 10009−10014.

(33) Hawkridge, A. M.; Pemberton, J. E. *J. Am. Chem. Soc.* **2002**, *125*, 624−625.

(34) Schalnat, M. C.; Hawkridge, A. M.; Pemberton, J. E. *J. Phys. Chem. C* **2011**, *115*, 13717−13724.

(35) Matz, D. L.; Schalnat, M. C.; Pemberton, J. E. *J. Am. Chem. Soc.* **2012**, *134*, 12989−12997.

(36) Matz, D. L.; Pemberton, J. E. *J. Phys. Chem. C* **2012**, *116*, 11548−11555.

(37) Dresselhaus, M. S.; Dresselhaus, G.; Eklund, P. C. *J. Raman Spectrosc.* **1996**, *27*, 351−371.

(38) Kuzmany, H.; Matus, M.; Burger, B.; Winter, J. *Adv. Mater.* **1994**, *6*, 731−745.

(39) Shinar, J.; Vardeny, Z. V.; Kafafi, Z. H. *Optical and Electronic Properties of Fullerenes and Fullerene-Based Materials*; M. Dekker: New York, 2000.

(40) Dresselhaus, M. S.; Dresselhaus, G.; Eklund, P. C. *Science of Fullerenes and Carbon Nanotubes*; Academic Press: San Diego, 1996.

(41) Nishinaga, J.; Horikoshi, Y. *J. Vac. Sci. Technol., B* **2010**, *28*, C3E10−C3E13.

(42) Kuzmany, H.; Pfeiffer, R.; Hulman, M.; Kramberger, C. *Philos. Trans. R. Soc., A* **2004**, *362*, 2375−2406.

(43) Mitch, M. G.; Lannin, J. S. *J. Phys. Chem. Solids* **1993**, *54*, 1801−1816.

(44) Akers, K. L.; Moskovits, M. *Thin Solid Films* **1995**, *257*, 204−210.

(45) Eklund, P. C.; Ping, Z.; Kai-An, W.; Dresselhaus, G.; Dresselhaus, M. S. *J. Phys. Chem. Solids* **1992**, *53*, 1391−1413.

(46) Tiani, D. J.; Pemberton, J. E. *Langmuir* **2003**, *19*, 6422−6429.

(47) Rao, A. M.; Zhou, P.; Wang, K.-A.; Hager, G. T.; Holden, J. M.; Wang, Y.; Lee, W. T.; Bi, X.-X.; Eklund, P. C.; Cornett, D. S.; Duncan, M. A.; Amster, I. J. *Science* **1993**, *259*, 955−957.

(48) Dong, Z.-H.; Zhou, P.; Holden, J. M.; Eklund, P. C.; Dresselhaus, M. S.; Dresselhaus, G. *Phys. Rev. B* **1993**, *48*, 2862−2865.
(49) Ferrari, A. C.; Robertson, J. *Phys. Rev. B* **2000**, *61*, 14095−14107.
(50) Wu, C. I.; Hirose, Y.; Sirringhaus, H.; Kahn, A. *Chem. Phys. Lett.* **1997**, *272*, 43−47.
(51) Baumgarten, M.; Gügel, A.; Gherghel, L. *Adv. Mater.* **1993**, *5*, 458−461.
(52) McGlashen, M. L.; Blackwood, M. E.; Spiro, T. G. *J. Am. Chem. Soc.* **1993**, *115*, 2074−2075.
(53) Zhang, Y.; Edens, G.; Weaver, M. J. *J. Am. Chem. Soc.* **1991**, *113*, 9395−9397.
(54) Haddon, R. C.; Hebard, A. F.; Rosseinsky, M. J.; Murphy, D. W.; Duclos, S. J.; Lyons, K. B.; Miller, B.; Rosamilia, J. M.; Fleming, R. M.; Kortan, A. R.; Glarum, S. H.; Makhija, A. V.; Muller, A. J.; Eick, R. H.; Zahurak, S. M.; Tycko, R.; Dabbagh, G.; Thiel, F. A. *Nature* **1991**, *350*, 320−322.
(55) Pichler, T.; Matus, M.; Kürti, J.; Kuzmany, H. *Phys. Rev. B* **1992**, *45*, 13841−13844.
(56) Winter, J.; Kuzmany, H. *Solid State Commun.* **1992**, *84*, 935−938.
(57) Tamor, M. A.; Vassell, W. C. *J. Appl. Phys.* **1994**, *76*, 3823−3830.
(58) Tai, F. C.; Lee, S. C.; Chen, J.; Wei, C.; Chang, S. H. *J. Raman Spectrosc.* **2009**, *40*, 1055−1059.
(59) McCulloch, D. G.; Prawer, S.; Hoffman, A. *Phys. Rev. B* **1994**, *50*, 5905−5917.
(60) McCulloch, D. G.; Prawer, S. *J. Appl. Phys.* **1995**, *78*, 3040−3047.
(61) Prawer, S.; Nugent, K. W.; Lifshitz, Y.; Lempert, G. D.; Grossman, E.; Kulik, J.; Avigal, I.; Kalish, R. *Diamond Relat. Mater.* **1996**, *5*, 433−438.
(62) Khalid, F. A.; Beffort, O.; Klotz, U. E.; Keller, B. A.; Gasser, P.; Vaucher, S. *Acta Mater.* **2003**, *51*, 4575−4582.
(63) Rao, A. M.; Eklund, P. C.; Hodeau, J. L.; Marques, L.; Nunez-Regueiro, M. *Phys. Rev. B* **1997**, *55*, 4766−4773.
(64) Kamarás, K.; Pekker, S.; Forró, L.; Tanner, D. B. *Chem. Phys. Lett.* **1998**, *295*, 279−284.
(65) Eklund, P. C.; Rao, A. M.; Zhou, P.; Wang, Y.; Holden, J. M. *Thin Solid Films* **1995**, *257*, 185−203.
(66) Krause, M.; Deutsch, D.; Janda, P.; Kavan, L.; Dunsch, L. *Phys. Chem. Chem. Phys.* **2005**, *7*, 3179−3184.
(67) Zhou, P.; Dong, Z.-H.; Rao, A. M.; Eklund, P. C. *Chem. Phys. Lett.* **1993**, *211*, 337−340.
(68) *CRC Handbook of Chemistry and Physics*, 87 ed.; CRC Press: Boca Raton, FL, 2006.
(69) Rosenberg, A.; DiLella, D. P. *Chem. Phys. Lett.* **1994**, *223*, 76−81.
(70) Chase, S. J.; Bacsa, W. S.; Mitch, M. G.; Pilione, L. J.; Lannin, J. S. *Phys. Rev. B* **1992**, *46*, 7873−7877.
(71) Garrell, R. L.; Herne, T. M.; Szafranski, C. A.; Diederich, F.; Ettl, F.; Whetten, R. L. *J. Am. Chem. Soc.* **1991**, *113*, 6302−6303.
(72) Duclos, S. J.; Haddon, R. C.; Glarum, S. H.; Hebard, A. F.; Lyons, K. B. *Solid State Commun.* **1991**, *80*, 481−484.
(73) Akers, K. L.; Cousins, L. M.; Moskovits, M. *Chem. Phys. Lett.* **1992**, *190*, 614−620.
(74) Chan, C. T.; Kamitakahara, W. A.; Ho, K. M.; Eklund, P. C. *Phys. Rev. Lett.* **1987**, *58*, 1528−1531.
(75) Purdie, D.; Bernhoff, H.; Reihl, B. *Surf. Sci.* **1996**, *364*, 279−286.
(76) Lu, X.; Grobis, M.; Khoo, K. H.; Louie, S. G.; Crommie, M. F. *Phys. Rev. B* **2004**, *70*, 115418.
(77) Lichtenberger, D. L.; Nebesny, K. W.; Ray, C. D.; Huffman, D. R.; Lamb, L. D. *Chem. Phys. Lett.* **1991**, *176*, 203−208.
(78) Weaver, J. H. *J. Phys. Chem. Solids.* **1992**, *53*, 1433−1447.
(79) Maxwell, A. J.; Brühwiler, P. A.; Arvanitis, D.; Hasselström, J.; Johansson, M. K. J.; Mårtensson, N. *Phys. Rev. B* **1998**, *57*, 7312−7326.
(80) Owens, D. W.; Aldao, C. M.; Poirier, D. M.; Weaver, J. H. *Phys. Rev. B* **1995**, *51*, 17068−17072.
(81) Yang, S. H.; Pettiette, C. L.; Conceicao, J.; Cheshnovsky, O.; Smalley, R. E. *Chem. Phys. Lett.* **1987**, *139*, 233−238.
(82) Ramm, M.; Ata, M.; Brzezinka, K. W.; Gross, T.; Unger, W. *Thin Solid Films* **1999**, *354*, 106−110.
(83) Ohno, T. R.; Chen, Y.; Harvey, S. E.; Kroll, G. H.; Weaver, J. H.; Haufler, R. E.; Smalley, R. E. *Phys. Rev. B* **1991**, *44*, 13747−13755.
(84) Taima, T.; Chikamatsu, M.; Bera, R. N.; Yoshida, Y.; Saito, K.; Yase, K. *J. Phys. Chem. B* **2003**, *108*, 1−3.
(85) Chen, L. J.; Song, Q. L.; Xiong, Z. H.; Huang, J. H.; He, F. *Sol. Energy Mater. Sol. Cells* **2011**, *95*, 1138−1140.